Research Article

Fateh Ali*, Muhammad Zahid, Basma Souayeh*, Farwa Asmat, and Chinedu Nwaigwe

Analytical and numerical investigation for viscoelastic fluid with heat transfer analysis during rollover-web coating phenomena

https://doi.org/10.1515/phys-2024-0024
received January 12, 2024; accepted April 03, 2024

Abstract: The current study theoretically and computationally analyses the viscoelastic Sisko fluids during the non-isothermal rollover web phenomenon. The mathematical modeling produces a system of partial differential equations, which we further simplify into ordinary differential equations through appropriate transformations. We have formulated the problem based on the lubrication approximation theory. The solution has been obtained with the perturbation method, and the outcomes are found in mathematical, tabular, and graphical forms that highlight the influence of pertinent parameters on velocity profiles, pressure gradients, flow rates per unit width, Nusselt number, pressure profile, temperature distributions, and other significant engineering quantities. Further, A comparative analysis between analytic and numerical solutions, utilizing the middefer method in the Maple environment, demonstrates reasonable agreement. Also, we observe that the fluid parameter significantly influences both velocity and temperature profiles. Moreover, the determination of a separation point 2.5000, accompanied by the observation of a maximum coating thickness of 0.6960. The enhancement in fluid heat transfer rate is approximately 5% compared to non-Newtonian fluid parameter values, with potential for further improvement by increasing the non-Newtonian parameter values. This comprehensive investigation offers valuable insights for practical implementation and future scholarly endeavors, with zero-order findings showcasing enhanced precision.

Keywords: Sisko fluid model, roll over web, analytic solution, temperature distribution, numeric computation

Nomenclature

H_0	nip region
$\frac{H}{H_0}$	coating thickness
R	roll radius (m)
U	velocity of the roll $\left(\frac{\mathrm{m}}{\mathrm{s}}\right)$
ρ	fluid density $\left(\frac{\mathrm{kg}}{\mathrm{m}^3}\right)$
λ	flow rate

1 Introduction

Fluids demonstrating non-Newtonian rheologies are frequently encountered in various domains, such as hydraulic fracturing, increased oil recovery, cleanup, and industrial processes [1–3]. Researchers have conducted numerous studies [4,5] to examine the characteristics of non-Newtonian fluids in different geometries, especially in the coating process [6]. Coating process has gained much attention in the last few decades for researchers, as it has many applications in the polymer industry. Coating is a procedure that involves continually applying liquid to a moving sheet to attain uniform fluid distribution onto the sheet. The term web is frequently used to refer to the sheet that will be coated, and webs can be made of several materials such as paper and paper board, fibers, fabrics, plastic fibers, textile fibers, metal foil, and cellulosic film. Benkreira *et al.* [7] examined coating flows extensively, focusing on four distinct categories: metered, gravure, free, and

*** Corresponding author: Fateh Ali,** College of Mathematics and System Sciences, Xinjiang University, Urumqi, 830046, China, e-mail: fatehalirana@xju.edu.cn
*** Corresponding author: Basma Souayeh,** Department of Physics, College of Science, King Faisal university, P. O. Box 400, Al-Ahsa, 31982, Saudi Arabia; Laboratory of Fluid Mechanics, Physics Department, University of Tunis El Manar Tunis 2092, Tunisia, e-mail: bsouayeh@kfu.edu.sa
Muhammad Zahid: Department of Mathematics, COMSATS University Islamabad, Abbottabad Campus, 22060, Abbottabad, Pakistan
Farwa Asmat: School of Mathematical Sciences, Peking University, Beijing 100871, P.R. China
Chinedu Nwaigwe: Department of Mathematics, Rivers State University, Port Harcourt, Nigeria

transfer coating flows. The field of coating technology has become of significant interest among researchers in recent decades due to its broad range of applications within the polymer field. Sofou and Mitsoulis [8] presented the theoretical analysis of rollover-web coating using power law, Bingham, and Herschel–Bulkley models. They simplified the resulting equations of motion through lubrication approximation theory (LAT) and calculated all the engineering quantities. They concluded that reducing the power-law index or increasing the Bingham number, leads to higher coating thickness, separation point (hence domain length), and volumetric flow rate. Zafar *et al.* [9] created a theoretical framework for an isothermal couple stress theory during the roll coating procedure (RCP). The RCP has been used in numerous industries, such as paper, producing plastic film, paperboard cellulosic film, textile fiber, metal foils, *etc*. In RCP, the space amongst the two revolving rolls is significantly smaller than the radii of the rolls. When the fluid passes through this narrow gap, it emerges as a thin liquid film. This film can be utilized for surface coating purposes. The fundamental determinant of the thickness and regularity of the coated film is the fluid flow occurring in a narrow gap between both rotating rolls. The thickness of the coating is generally found by the spacing between neighboring rolls and the respective speeds at which they operate. As mentioned above, the procedure can generate various final products. Several commonly employed coating technologies include metering roll coating, reverse roll coating, extrusion coating, forward roll coating (FRC), kiss roll coating, blade coating, withdrawal coating, rollover web, and free coating [10]. However, thus far, less attention has been given to the rollover-web coating procedure [11]. This procedure has significant practical applications in engineering, particularly in industries involving the manufacturing of thin films, such as in electronics, optics, and packaging.

Middleman first introduced the principle of rollover-web coating in their work in 1975 [12]. They developed a mathematical model and investigated the problem when the roll and sheet are moving at the same speed by assuming a small roll curvature in the same direction. They simplified the constitutive equations of motion for Newtonian fluid, power-law fluid, and viscoelastic fluid model using lubrication theory and calculated the engineering quantities analytically for both Newtonian and non-Newtonian fluids and obtained numerical results for viscoelastic fluids using a perturbation technique. Decré *et al.* [13] conducted experimental investigations on the meniscus shape in FRC. The hydrodynamics of a non-Newtonian commercial coating were examined by Lecuyer *et al.* [14] by applying the FRC model. Ali *et al.* [15] examined the behavior of a non-Newtonian fluid coating among two reversely revolving rolls. They found that the velocity ratio parameters and Weissenberg number play important roles in controlling the pressure gradient and pressure distribution. Zahid *et al.* [16] examined the process of RCP for the non-Newtonian thin film using two rolls revolving in the same direction. Roll coating is a manufacturing technique that involves the creation of a thin liquid film over a continuous web or substrate by utilizing multiple rotating rolls. A theoretical examination of rollover thin layer development under LAT was analyzed by Manzoor *et al.* [17]. They found that the transport properties are affected due to couple stress and velocity decreases because of increase in applied couple stress. The study conducted by Decré *et al.* [13] focused on examining roll coating flows within the framework of the lubrication approximation. The researchers employed a viscocapillary model to understand the flow dynamics between rolls with deformable and rigid characteristics. In their study, Gaskell *et al.* [18] employed particle imaging methods and optical segmenting in conjunction with a color injection to investigate the precise fluid dynamics of the meniscus during reverse and FRC processes. The study conducted by Atif *et al.* [19] involved an analysis of the rollover-web coating process on a moving web. They employed the LAT and utilized a micropolar fluid for their investigation. They concluded that the pressure and pressure gradient in the nip region increase with the increase in the coupling numbers and microrotation parameters. Researchers examined many fluid models based on specific material characteristics, including Casson fluid, Oldroyd-B, second-grade, couple stress, third-grade, and Jeffrey fluid. However, so far, no effort is presented which quantify the impact of Sisko fluid (viscoelastic fluid) during the rollover-web coating procedure. It was named after Sisko in 1958 [20]. The potential of the model under research to effectively depict the phenomena of shear-thickening and shear-thinning is one of the primary reasons for it to be of such considerable importance. These phenomena include viscous and power-law fluids as specific examples. The broad range of applications of viscoelastic fluid such as in the oil and gas industry, where drilling fluids, which are often viscoelastic, are used to lubricate drill bits, carry rock cuttings to the surface, and maintain wellbore stability by exerting pressure on the formation. In biomedical engineering, viscoelastic fluids are utilized in tissue engineering and drug delivery systems due to their ability to mimic biological tissues mechanical behavior. Moreover, in industries like food processing and cosmetics, these fluids are employed to control texture, stability, and flow properties in products such as sauces, creams, and gels. This model provides an accurate description of the flow behavior of greases, which exhibit higher viscosities at lower shear rates and lower viscosities at higher shear rates [21].

Over time, analytical methodologies have demonstrated their efficacy as valuable instruments for comprehending the intricacies inherent in non-Newtonian fluids. Numerous methods have been established to approximate solutions for problems involving non-Newtonian fluids. These methods include the perturbation method (PM), the variational iteration method, the Adomian decomposition method (ADM), the homotopy PM, the homotopy analysis method (HAM), the optimal HAM, and many more. These methods have been widely applied in various industries and technological fields. The analytic solution for the considered problem has been derived with the assistance of the regular PM [22].

From the above cited literature, it is evident that thus far, no attempt has been made to model roll coating process using Sisko fluid model constitutive equations. The objective of this study is to investigate the flow behavior of the Sisko fluid. Specifically, we focus on the rollover web coating process and give analytical and numeric solutions. This study has significant physical quantities, such as the velocity profile, separation points, pressure profile, Nusselt number, streamlines, volume flow rate, uniform film thickness, and temperature distribution. The PM provides solutions for the pressure gradient, velocity profile, flow rate, and temperature distribution. The numeric technique called regular false position has been used to find the coating thickness. This study presents the consequences of several parameters on various quantities through graphs and tables.

The structure of this study is outlined as follows: The subsequent sections cover the fundamental flow equation; then, the mathematical formulation and the solution to the flow problem are outlined. Subsequently, the perturbation and numerical methods are discussed. Further, the graphical results and discussion are presented. Finally, conclusion is offered.

2 Fundamental equations

The equations controlling the conservation of mass and momentum for non-isothermal, incompressible Sisko fluid, subject to the influence of body forces, can be expressed as follows [23]:

$$\mathrm{div}\mathbf{u} = 0, \tag{1}$$

$$\mathrm{div}\mathbf{T} = \rho\frac{\mathrm{d}\mathbf{u}}{\mathrm{d}t} + \rho\mathbf{f}, \tag{2}$$

$$\mathbf{T} = -p\mathbf{I} + \boldsymbol{\tau}. \tag{3}$$

The energy equation can be derived from the first law of thermodynamics, which is a fundamental principle that states the equivalence between the heat contributed to a system and the change in its internal energy, in addition to the work performed. The simplified form of the energy equation can be stated as follows [24]:

$$\rho C_{\mathrm{p}}\left(\frac{\mathrm{D}\theta}{\mathrm{D}t}\right) = k\nabla^2\theta + \boldsymbol{\tau}\cdot\nabla\mathbf{V}, \tag{4}$$

where $\mathbf{V}$ stands for the velocity vector, $\mathbf{f}$ shows the body force, $\mathbf{I}$ is the identity tensor, ρ is the density, p is the hydrodynamic pressure, $\boldsymbol{\tau}$ is the Cauchy stress tensor, and $\mathrm{d}/\mathrm{d}t$ signifies the material time derivative specified by

$$\frac{\mathrm{d}\mathbf{V}}{\mathrm{d}t} = \frac{\partial\mathbf{V}}{\partial t} + (\mathbf{V}\cdot\nabla)\mathbf{V}. \tag{5}$$

The constitutive equation that governs the behavior of an incompressible Sisko fluid is defined as follows, as stated in previous literature [20,24,25]:

$$\boldsymbol{\tau} = \left[a + b\left(\sqrt{\frac{1}{2}\mathbf{A}_1^2}\right)^{n-1}\right]\mathbf{A}_1, \tag{6}$$

where a and b represent the material constants and the variable n serves as the fluid behavior index.

The rate of deformation tensor $\mathbf{A}_1$ in Eq. (5) is defined by

$$\mathbf{A}_1 = \mathbf{L} + \mathbf{L}^T, \tag{7}$$

with

$$\mathbf{L} = \mathrm{grad}\mathbf{V}. \tag{8}$$

It should be noted that for $a = \mu$ and $b = 0$, Eq. (6) reduces to the equation of a linearly viscous Newtonian fluid and reduces to power-law fluid model if $a = 0$.

3 Problem formulation

Assume for the moment that a non-isothermal steady-state operation is coating a fluid with pair stress on a sheet. The radius of the rolls is denoted as R, and it is revolving counterclockwise with an angular velocity represented by ω, resulting in a linear velocity denoted as $U_2 = \omega R$. The web or sheet is toward the positive x-direction with a constant velocity U_1. The dimension of the space between the roll and web in the smallest separation area, also known as the nip area, is denoted as H_0. The polymer undergoes initial contact with the planar surface at a specific point $x = -\eta_{\mathrm{b}}$, as depicted in Figure 1. Moreover, it is assumed that the flow is symmetrical $H_0/R \ll 1$, so it can be approximated as occurring between two parallel borders in the vicinity of the nip zone and extending in both directions. Based on this assumption, it may be concluded that the lubrication theory holds true in the vicinity of the nip zone.

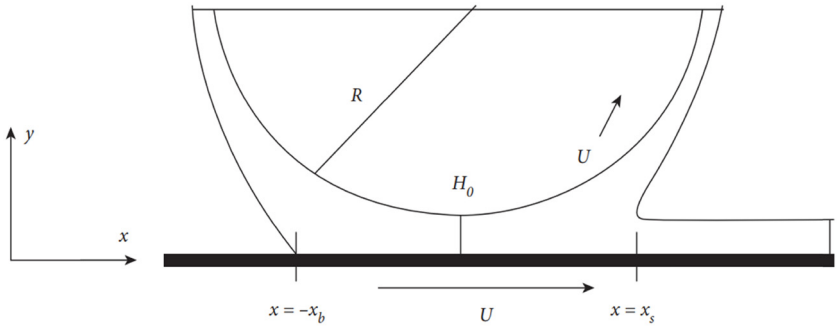

Figure 1: Structure of examined model.

The velocity field for two-dimensional fluid flow is specified by

$$\mathbf{V} = [u(x, y), v(x, y)]. \tag{9}$$

In the circumstances previously indicated, the $\sigma(x)$ variable denoted as "height between roll and the web" is represented by the term and is explicitly defined as.

$$\sigma(x) = H_0 + R - (R^2 - x^2)^{\frac{1}{2}}, \tag{10}$$

Eq. (10), under the supposition $H_0/R \ll 1$, reduces to

$$\sigma(x) = H_0\left(1 + \frac{x^2}{2H_0R}\right). \tag{11}$$

An order of magnitude study is carried out to determine the typical ranges for velocity and pressure. To conduct this evaluation, we use the following measures for y, x, and u.

$$x \sim L_c, \rightarrow u \sim U_1, \rightarrow y \sim H_0, \tag{12}$$

By utilizing Eq. (1) in conjunction with Eq. (12), we can deduce

$$\frac{v_c}{U_1} \sim \frac{H_0}{L_c} \ll 1, \tag{13}$$

This demonstrates that the transversal velocity v is of a lesser order of magnitude than the longitudinal velocity u, possessing the standard length provided by $L_c = \sqrt{2RH_0}$. The standard pressure is attained by utilizing Eq. (2) that generates a dominant equilibrium between the viscous and pressure components, leading to the subsequent formulation:

$$p \sim \sqrt{\frac{2R}{H_0}}\frac{\mu U_1}{H_0}, \tag{14}$$

in the equation mentioned above, the variable represents the distance from the centre line to the surface of the roll. By utilizing Eq. (9), it is possible to express Eqs. (1)–(6) in their component form.

$$\frac{\partial u}{\partial x} + \frac{\partial v}{\partial y} = 0, \tag{15}$$

$$\rho\left(u\frac{\partial u}{\partial x} + \frac{\partial u}{\partial y}\right) = -\frac{\partial p}{\partial x} + \frac{\partial \tau_{xy}}{\partial y} + \frac{\partial \tau_{xx}}{\partial x}, \tag{16}$$

$$\rho\left(u\frac{\partial v}{\partial x} + \frac{\partial v}{\partial y}\right) = -\frac{\partial p}{\partial y} + \frac{\partial \tau_{yx}}{\partial x} + \frac{\partial \tau_{yy}}{\partial y}, \tag{17}$$

$$\begin{aligned} C_p\rho\left(u\frac{\partial \theta}{\partial x} + v\frac{\partial \theta}{\partial y}\right) &= k\left(\frac{\partial^2\theta}{\partial x^2} + \frac{\partial^2\theta}{\partial y^2}\right) + \tau_{xx}\frac{\partial u}{\partial x} \\ &\quad + \tau_{xy}\left(\frac{\partial u}{\partial y} + \frac{\partial v}{\partial x}\right) + \tau_{yy}\frac{\partial v}{\partial y}, \end{aligned} \tag{18}$$

where

$$\begin{aligned} \tau_{xx} &= \left[a + b\left(\sqrt{2\left(\frac{\partial u}{\partial x}\right)^2 + \left(\frac{\partial u}{\partial y} + \frac{\partial v}{\partial x}\right)^2 + 2\left(\frac{\partial v}{\partial y}\right)^2}\right)^{n-1}\right] \\ &\quad \times \left(2\frac{\partial u}{\partial x}\right), \end{aligned} \tag{19}$$

$$\begin{aligned} \tau_{xy} &= \tau_{yx} \\ &= \left[a + b\left(\sqrt{2\left(\frac{\partial u}{\partial x}\right)^2 + \left(\frac{\partial u}{\partial y} + \frac{\partial v}{\partial x}\right)^2 + 2\left(\frac{\partial v}{\partial y}\right)^2}\right)^{n-1}\right] \\ &\quad \times \left(\frac{\partial u}{\partial y} + \frac{\partial v}{\partial x}\right), \end{aligned} \tag{20}$$

$$\begin{aligned} \tau_{yy} &= \left[a + b\left(\sqrt{2\left(\frac{\partial u}{\partial x}\right)^2 + \left(\frac{\partial u}{\partial y} + \frac{\partial v}{\partial x}\right)^2 + 2\left(\frac{\partial v}{\partial y}\right)^2}\right)^{n-1}\right] \\ &\quad \times \left(2\frac{\partial v}{\partial y}\right). \end{aligned} \tag{21}$$

3.1 LAT analysis

Scientists and engineers often simplify mathematically determined models to provide useful approximations

when confronted with complex physical systems. The objective of this procedure is to produce an approximation. The successful implementation of simplifications requires a comprehensive understanding of the physical system, including all dimensions of the fluxes, forces, velocities, and other components that are involved in the problem. To derive these simplifications, we disregard the less significant terms from the governing equations and only consider the more significant ones. Since there is only a small amount of roll separation in the nip region, we will start with the LAT argument. According to the information depicted in Figure 1, it can be observed that in the vicinity of the nip and extending in both directions along the $\pm x$-directions, the surfaces of the rolls are almost parallel when $H_0 \ll R$. Based on the above information, it is reasonable to accept that the flow is almost parallel, so that $v \ll u$ and $\frac{\partial}{\partial x} \ll \frac{\partial}{\partial y}$. Using this approximation, Eqs. (15)–(21) reduces to

$$0 = -\frac{\partial p}{\partial x} + \frac{\partial \tau_{xy}}{\partial y}, \tag{22}$$

$$0 = -\frac{\partial p}{\partial y} + \frac{\partial \tau_{yy}}{\partial y}, \tag{23}$$

where

$$\tau_{xy} = \left[a + b\left(\sqrt{\left(\frac{\partial u}{\partial y}\right)^2}\right)^{n-1}\right]\left(\frac{\partial u}{\partial y}\right), \tag{24}$$

$$\tau_{yy} = 0. \tag{25}$$

Substituting Eq. (24) in Eq. (22), also, it has been found that $\frac{\partial p}{\partial y} = 0$, which further implies that $p = p(x)$ only; therefore, Eq. (22) takes the following form:

$$a\frac{\delta^2 u}{\delta y^2} + nb\left(\frac{\delta u}{\delta y}\right)^{n-1}\frac{\delta^2 u}{\delta y^2} = \frac{\delta p}{\delta x}, \tag{26}$$

and

$$k\frac{\partial^2 \theta}{\partial y^2} + \left(a\frac{\partial u}{\partial y} + b\left(\frac{\partial u}{\partial y}\right)^n\right)\left(\frac{\partial u}{\partial y}\right) = 0, \tag{27}$$

and suitable boundary conditions (BCs) are [6]

$$\begin{cases} u = U, v = 0 \quad \text{on} \quad y = \sigma(x), \\ \tau_{xy} = 0, v = 0 \quad \text{on} \quad y = 0. \end{cases} \tag{28}$$

3.2 Dimensionless equations

Within this area, we shall present the dimensionless controlling equations crucial for resolving the non-isothermal calendaring procedure. We develop the subsequent non-dimensional parameters by expanding upon the previous research utilizing lubrication theory [6].

$$\begin{aligned} x^* &= \frac{x}{\sqrt{2RH_0}}, u^* = \frac{u}{U}, y^* = \frac{y}{H_0}, P^* = \sqrt{\frac{H_0}{2R}}\frac{PH_0}{aU} \\ Q^* &= \frac{Q}{2UH_0}, \tau_{xy}{}^* = \frac{\tau_{xy}H_0}{aU}, \sigma^*(x^*) = \frac{\sigma(x)}{H_0} = 1 + x^2, \end{aligned} \tag{29}$$

employing non-dimensional variables given in Eq. (29) in Eqs. (26) and (27) after eliminating the "–" sign yield

$$\frac{\mathrm{d}^2 u}{\mathrm{d}y^2} + n\beta\left(\frac{\mathrm{d}u}{\mathrm{d}y}\right)^{n-1}\left(\frac{\mathrm{d}^2 u}{\mathrm{d}y^2}\right) = \frac{\mathrm{d}p}{\mathrm{d}x}, \tag{30}$$

and

$$\frac{\mathrm{d}^2}{\mathrm{d}y^2}\theta(y) + \beta\mathrm{Br}\left(\frac{\mathrm{d}}{\mathrm{d}y}u(y)\right)^{n+1} + \mathrm{Br}\left(\frac{\mathrm{d}}{\mathrm{d}y}u(y)\right)^2 = 0. \tag{31}$$

The volumetric flow rate in integral form is defined as follows:

$$Q = 1 + \lambda^2 = \int_0^{h(x)} u\mathrm{d}y, \tag{32}$$

where $h(x) = 1 + \frac{x^2}{2}$.

4 Analytic solution for the limit $\beta \ll 1$

To find an analytic solution of Eq. (30), the conventional perturbation approach is utilized. The regular PM is an important method for estimating solutions to differential equations, especially when the exact solutions cannot be explicitly expressed or are difficult to calculate. It is a frequently employed analytical methodology in the fields of mathematics and engineering. The perturbation technique relies on the assumption of a small parameter, typically represented as β, which perturbs a system from a state where the solution is known. Now, introducing β as the perturbative parameter, we establish the subsequent series expansions

$$u(x,y) = \sum_{k=0}^{\infty} u_k(x,y)\beta^k = u_0(x,y) + \beta u_1(x,y) + \dots, \tag{33}$$

$$\theta(x,y) = \sum_{k=0}^{\infty} \theta_k(x,y)\beta^k = \theta_0(x,y) + \beta\theta_1(x,y) + \dots, \tag{34}$$

where the coefficient functions $u_0(x, y)$, $u_1(x, y)$, $\theta_0(x, y)$, $\theta_1(x, y)$, ... are independent of β.

$$\frac{\mathrm{d}p}{\mathrm{d}x} = \sum_{k=0}^{\infty}\frac{\mathrm{d}p_k}{\mathrm{d}x}\beta^k = \frac{\mathrm{d}p_0}{\mathrm{d}x} + \beta\frac{\mathrm{d}p_1}{\mathrm{d}x} + \dots, \tag{35}$$

$$p(x) = \sum_{k=0}^{\infty} p_k \beta^k = p_0(x) + \beta p_1(x) + \dots , \tag{36}$$

$$Q = \sum_{k=0}^{\infty} Q_0 \beta^k = Q_0 + \beta Q_1 + \dots , \tag{37}$$

$$\lambda = \sum_{k=0}^{\infty} \lambda_k \beta^k = \lambda_0 + \beta \lambda_1 + \dots , \tag{38}$$

By substituting the relationships (33)–(38) in Eqs. (30) and (31), and grouping words with the same powers of β, we can derive zeroth-order and first-order problems. These problems and their corresponding solutions are presented in the subsequent sections.

4.1 Zeroth-order problem and its solution

By comparing the terms that are independent of β in Eq. (33), we may identify the zeroth-order problem.

$$\frac{\mathrm{d}^2}{\mathrm{d}y^2} u_0(y) - \frac{\mathrm{d}}{\mathrm{d}x} p_0(x) = 0, \tag{39}$$

$$\lambda = \int_0^{h(x)} u_0 \mathrm{d}y. \tag{40}$$

With the inclusion of the zeroth-order boundary conditions that are in agreement

$$u_0(0) = 1, \quad u_0(\sigma) = 1. \tag{41}$$

The solution to Eq. (39) subject to the conditions specified in Eq. (41) is provided as follows:

$$u_0(y) = \frac{\left(\frac{\mathrm{d}}{\mathrm{d}x} P_0(x)\right) y^2}{2} - \frac{\sigma \left(\frac{\mathrm{d}}{\mathrm{d}x} P_0(x)\right) y}{2} + 1. \tag{42}$$

The measurement of the pressure distribution in Eq. (42) can be achieved by applying the concept of conservation of mass. This pressure distribution exhibits the corresponding pattern.

$$\frac{\mathrm{d}p_0}{\mathrm{d}x} = 12 \frac{\sigma(x) - \lambda_0}{(\sigma(x))^3}. \tag{43}$$

By substituting Eq. (43) in Eq. (42), it is possible to express the velocity distribution of zero-order as follows:

$$u_0(x, y) = 1 + 6\left(\frac{\sigma - \lambda_0}{h^3}\right)(y^2 - \sigma y). \tag{44}$$

Based on the assumption above, on which the above expression is derived also enables us to identify that the separation point (the point where the liquid splits in two parts). At the separation point the velocity must vanish by symmetric requirements. Therefore, based on Eq. (43), we can express

$$x_0 = \sqrt{3\lambda_0 - 1}. \tag{45}$$

The integral form of Eq. (43) can be written in the following way:

$$p_0 = 12 \int_{x_s}^{x} \frac{\sigma(x) - \lambda_0}{\sigma(x)^3}, \tag{46}$$

where x_s is the value to be found at $p = 0$. The determination of the pressure at the separation point can be achieved through the application of the first integral of Eq. (43), under the assumption that $x_b \to -\infty$

$$\begin{aligned} p_0 = {} & \frac{(6 - (9/2)\lambda_0)x}{1 + (x^2/2)} - \frac{3\lambda_0 x}{(1 + (x^2/2))^2} \\ & + \left(\frac{12}{\sqrt{2}} - \frac{9\lambda_0}{\sqrt{2}}\right) \tan^{-1} \frac{x}{\sqrt{2}} + \frac{6\pi}{\sqrt{2}} \left(1 - \frac{3\lambda_0}{4}\right). \end{aligned} \tag{47}$$

The most basic dynamic model of the separation zone is predicated on the premise that the film divides at the precise location where $u_0 = 0$ and $p_0 = 0$, specifically, velocity, pressure, and temperature are satisfied.

Consequently, as mentioned earlier, the equation transforms into a transcendental equation in λ_0, which requires the utilization of a numerical method known as the regula falsi position method to achieve its solution with a predetermined level of 10^{-10}.

The zero-order flow rate, accurate up to five decimal places, is determined to be $\lambda_0 = 1.3015$. The corresponding residual error in this scenario is calculated to be −0.00046. It is important to note that the coating thickness, as mentioned earlier, is attained precisely at the separation point $x_0 = 2.4102$. It is noteworthy that the aforementioned zero-order outcomes exhibit higher accuracy, as determined by Greener and Middleman [6].

4.2 First-order problem and its solution

When examining and contrasting concepts, it is essential to consider the independence from certain constraints or limitations. In Eq. (33), we encounter the subsequent first-order problem

$$\frac{\mathrm{d}^2}{\mathrm{d}y^2} u_1(y) + n\left(\frac{\mathrm{d}^2}{\mathrm{d}y^2} u_0(y)\right)\left(\frac{\mathrm{d}}{\mathrm{d}y} u_0(y)\right)^{n-1} = \left(\frac{\mathrm{d}}{\mathrm{d}x} p_1(x)\right), \tag{48}$$

after the substitution of the solution of zeroth-order from Eq. (42), we have the following first-order problem:

$$\frac{d^2}{dy^2}u_1(y) + n\left(\left(\frac{d}{dx}p_0(x)\right)y - \frac{\sigma\left(\frac{d}{dx}p_0(x)\right)}{2}\right)^{n-1}\left(\frac{d}{dx}p_0(x)\right) = \frac{d}{dx}p_1(x), \tag{49}$$

and the boundary conditions (BCs) are

$$u_1(0) = 0, u_1(\sigma) = 0, \tag{50}$$

the first-order solution along with BCs is:

$$u_1(y) = \frac{(y-\sigma)\left(\left(y^4 - 2y^3\sigma + \frac{7}{4}y^2\sigma^2 - \frac{3}{4}y\sigma^3 + \frac{3}{16}\sigma^4\right)\left(\frac{d}{dx}p_0(x)\right)^5 - 3\frac{d}{dx}p_1(x)\right)y}{6}, \tag{51}$$

$$\lambda_1 = \int_0^{\sigma(x)} u_1 dy, \tag{52}$$

$$\frac{dp_1}{dx} = -\frac{12\left(7\lambda_1\sigma^8 + 3,888\lambda_0^5 - 19,440\lambda_0^4\sigma + 38,880\lambda_0^3\sigma^2 - 38,880\lambda_0^2\sigma^3 + 19,440\lambda_0\sigma^4 - 3,888\sigma^5\right)}{7\sigma^{11}}. \tag{53}$$

$$u_2(y) = \frac{1}{2}\left((y-\sigma)\left(\left(y^4 - \frac{3}{2}y^3\sigma + y^2\sigma^2 - \frac{1}{4}y\sigma^3 + \frac{1}{16}\sigma^4\right)\left(y^4\frac{5}{2}y^3\sigma + \frac{5}{2}y^2\sigma^2 - \frac{5}{4}y\sigma^3 + \frac{5}{16}\sigma^4\right)\left(\frac{d}{dx}p_0(x)\right)^9 - \frac{5\left(y^2 - \frac{1}{2}y\sigma + \frac{1}{4}\sigma^2\right)\left(\frac{d}{dx}p_1(x)\right)\left(y^2 - \frac{3}{2}y\sigma + \frac{3}{4}\sigma^2\right)\left(\frac{d}{dx}p_0(x)\right)^4}{3} + \frac{d}{dx}p_2(x)\right)y\right). \tag{56}$$

4.3 Second-order problem and its solution

By comparing the terms derived from Eq. (33), we may establish a second-order problem with the corresponding BCs

$$\frac{d^2}{dy^2}u_2(y) + 5\left(\frac{d}{dy}u_0(y)\right)^4\left(\frac{d^2}{dy^2}u_1(y)\right) + 20\left(\frac{d}{dy}u_0(y)\right)^3\left(\frac{d}{dy}u_1(y)\right)\left(\frac{d^2}{dy^2}u_0(y)\right) = \frac{d}{dx}p_2(x), \tag{54}$$

$$u_2(0) = 0, u_2(\sigma) = 0. \tag{55}$$

After simplifications, the second solution is

The research is not yet complete because the connection between the non-dimensional separation point x_s and the flow rate λ needs to be assessed for first and second-order solutions. Figure 1 specifies that the web splits equally, and, subsequently, the segregation point is $(x_s, \sigma(x_s)/2)$. The pressure and velocity profiles are both zero or very close to it. The roll and the sheet are supposed to be substituted at the same frequency. It causes separation points x_s depending upon the non-dimensional coating thickness λ. So, a similar process can be assumed for the zeroth-order system, and we can calculate the value of the separation points and volumetric flow rate for the first- and second-order problems.

5 Temperature distribution

The dimensionless form of temperature distribution is

$$\frac{d^2}{dy^2}\theta(y) + Br\beta\left(\frac{d}{dy}u(y)\right)^{n+1} + Br\left(\frac{d}{dy}u(y)\right)^2 = 0. \tag{57}$$

The suitable boundary condition for Eq. (57) is

$$\theta(0) = 0, \quad \theta(\sigma) = 1. \tag{58}$$

By employing Eq. (34), we get

$$\frac{d^2}{dy^2}\theta_0(y) + \beta\left(\frac{d^2}{dy^2}\theta_1(y)\right) + \beta^2\left(\frac{d^2}{dy^2}\theta_2(y)\right) + Br\left(\frac{d}{dy}u_0(y) + \beta\left(\frac{d}{dy}u_1(y)\right) + \beta^2\left(\frac{d}{dy}u_2(y)\right)\right)^2 + Br\beta\left(\frac{d}{dy}u_0(y) + \beta\left(\frac{d}{dy}u_1(y)\right) + \beta^2\left(\frac{d}{dy}u_2(y)\right)\right)^{n+1} = 0, \tag{59}$$

By substituting $n = 4$, and comparing the similar power of β on both sides, we obtain

$$\frac{d^2}{dy^2}\theta_0(y) + Br\left(\frac{d}{dy}\theta_0(y)\right)^2 = 0, \tag{60}$$

$$\frac{d^2}{dy^2}\theta_1(y) + 2\mathrm{Br}\left(\frac{d}{dy}u_0(y)\right)\left(\frac{d}{dy}u_1(y)\right) + \mathrm{Br}\left(\frac{d}{dy}u_0(y)\right)^5 = 0, \tag{61}$$

$$\frac{d^2}{dy^2}\theta_2(y) + \mathrm{Br}\left(2\left(\frac{d}{dy}u_0(y)\right)\left(\frac{d}{dy}u_2(y)\right) + \left(\frac{d}{dy}u_1(y)\right)^2\right) + 5\mathrm{Br}\left(\frac{d}{dy}u_0(y)\right)^4\left(\frac{d}{dy}u_1(y)\right) = 0. \tag{62}$$

5.1 Zeroth-order problem and its solution

The zeroth-order BVP is

$$\frac{d^2}{dy^2}\theta_0(y) + \mathrm{Br}\left(\frac{d}{dy}\theta_0(y)\right)^2 = 0. \tag{63}$$

BCs are

$$\theta_0(0) = 0, \theta_0(\sigma) = 1, \tag{64}$$

$$\theta_0(y) = -\frac{288y\left(-\frac{8\left(-\frac{x^2}{2}+Q-1\right)^2\mathrm{Br}\sigma^4}{3} + \frac{8(x^2+2)\left(-\frac{x^2}{2}+Q-1\right)^2\mathrm{Br}\sigma^3}{3} - (x^2+2)^2\left(-\frac{x^2}{2}+Q-1\right)^2\mathrm{Br}\sigma^2 + \left(x^4+\left(4-\frac{8y}{3}\right)x^2+\frac{8y^2}{3}-\frac{16y}{3}+4\right)y\left(-\frac{x^2}{2}+Q-1\right)^2\mathrm{Br}\sigma - \frac{(x^2+2)^6}{288}\right)}{(x^2+2)^6\sigma}. \tag{65}$$

5.2 First- and second-order problems

The first- and second-order problems are

$$\frac{d^2}{dy^2}\theta_1(y) + 2\mathrm{Br}\left(\frac{d}{dy}u_0(y)\right)\left(\frac{d}{dy}u_1(y)\right) + \mathrm{Br}\left(\frac{d}{dy}u_0(y)\right)^5 = 0. \tag{66}$$

BCs

$$\theta_1(0) = 0, \theta_1(\sigma) = 0, \tag{67}$$

$$\frac{d^2}{dy^2}\theta_2(y) + \mathrm{Br}\left(2\left(\frac{d}{dy}u_0(y)\right)\left(\frac{d}{dy}u_2(y)\right) + \left(\frac{d}{dy}u_1(y)\right)^2\right) + 5\mathrm{Br}\left(\frac{d}{dy}u_0(y)\right)^4\left(\frac{d}{dy}u_1(y)\right) = 0. \tag{68}$$

BCs are

$$\theta_2(0) = 0, \theta_2(\sigma) = 0. \tag{69}$$

Therefore, the comprehensive solution for the velocity profile, temperature distribution, pressure gradient, pressure profile, and flow rate may be derived by merging the solutions of zeroth- and first-order problems.

6 Operating variables

After establishing the pressure distribution, velocity, temperature profile, and pressure gradient, it becomes feasible to calculate all other pertinent engineering parameters relatively easily. The procedure for determining the operating variables is as follows:

6.1 Coating thickness

It can be shown that the web thickness H_b at the entrance is

$$H_b = 1 + \frac{x_b^2}{2}. \tag{70}$$

We can express the volumetric flow rate $Q = 2UH$, since we assume the fluid splits up equally to coat the plane and roll.

$$\frac{H}{H_0} = \frac{\lambda}{2}. \tag{71}$$

This provides the resultant coating thickness upon departure in a non-dimensional representation.

6.2 Roll separating force

The force of roll separation F is given by

$$F = \int_{-\infty}^{x_s} p(x)dx, \tag{72}$$

where $F = (\bar{F}H_0/\eta_0 URW), \bar{F}$ stands for the dimensional form of the force of the roll separation per unit width W.

6.3 Power contribution

The power transmitted to the fluid by the roll is calculated by integrating the product of shear stress and the roll surface speed over the roll surface, which is subsequently produced by setting $\overline{y} = H_0$ it as

$$p_w = \int_{-\infty}^{x_s} \tau_{xy}(x, 1)dx, \tag{73}$$

where $p_w = (\overline{p_w}/\eta_0 U^2 W)$ is the non-dimensional power and $\tau_{xy} = \overline{\tau_{xy}} H_0/\eta_0 U$ is the non-dimensional stress tensor given by Eq. (24).

6.4 Nusselt number

The Nusselt number can be defined as follows:

$$\mathrm{Nu} = \left| \frac{\partial \theta}{\partial y} \right|_{y=\sigma}. \tag{74}$$

7 Numerical solution *via* middefer method

Before discussing the physical quantities parametrically, comparing approximate and numerical solutions is necessary to validate them. Various numerical techniques can be used to accomplish this. Palencia *et al.* [26,27] used Matlab and Runge Kutta methods to validate analytical solutions for the Eyring–Powell fluid and the Darcy–Forchheimer fluid flow. We utilize the Maple program, which is a practical tool that offers complex numerical approaches, for our numerical validation. We can develop a helpful program with straightforward declarations using this piece of software, which enables us to solve the problems associated with boundary value problems (BVP). Automatic identification of the problem (BVP) type is followed by applying the suitable algorithm. In our study, the method used is the middefer method [28,29], a technique of midpoint that uses enhancement schemes. Furthermore, the numerical method offers a beneficial approach through the continuation technique that modifies the coefficient of the second-order derivative in the equation. As an outcome, selecting the suitable number of max mesh [30] significantly diminishes the global error. It is an effective way to improve the accurateness of the solution.

7.1 Comparison of analytical and numerical computations

The analytical outcomes attained in Section 4 for the velocity profile during the rollover web coating process are now compared with the numerical solution for an involved material parameter β (Sisko fluid parameter). Numerical

Table 1: Compression among Newtonian, analytic, and numeric solutions for velocity at $\beta = 0.01$

y	Newtonian solution	Analytical solution	Numerical solution	Absolute error
0	1	1	1.0000	1.11022×10^{-16}
0.1	1.16281	1.16376	1.16645	0.00269
0.2	1.28944	1.29691	1.30139	0.00447
0.3	1.37989	1.39382	1.40008	0.00625
0.4	1.43416	1.45232	1.45983	0.00750
0.5	1.45225	1.47184	1.47978	0.00793
0.6	1.43416	1.45232	1.45983	0.00750
0.7	1.37989	1.39382	1.40008	0.00625
0.8	1.28944	1.29691	1.30139	0.00447
0.9	1.16281	1.16376	1.16645	0.00269
1.0	1	1	1.0000	1.11022×10^{-16}

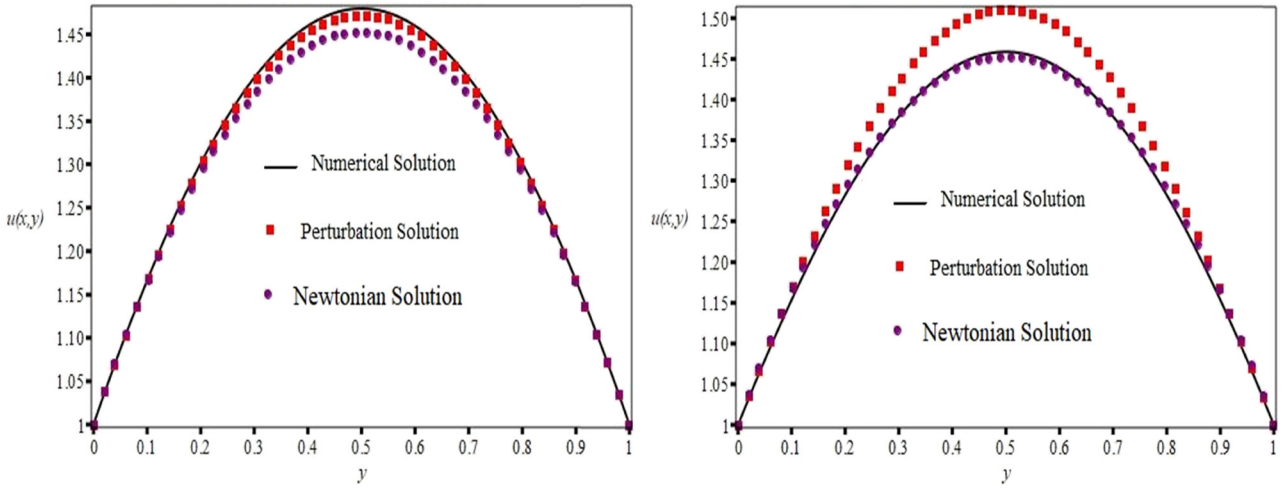

Figure 2: The variation in the analytic and numerical solutions for numerous values of the involved parameter.

Table 2: Compression among Newtonian, analytic, and numeric solutions for velocity at $\beta = 0.03$

y	Newtonian solution	Analytical solution	Numerical solution	Absolute error
0	1	1	1.0000	4.440892×10^{-16}
0.1	1.16281	1.16566	1.15353	0.01213
0.2	1.28944	1.31187	1.28218	0.02969
0.3	1.37989	142170	1.37908	0.04262
0.4	1.43416	1.48864	1.43863	0.05001
0.5	1.45225	1.51102	1.45857	0.05244
0.6	1.43416	1.48864	1.43863	0.05001
0.7	1.37989	1.42170	1.37908	0.04262
0.8	1.28944	1.31187	1.28218	0.02969
0.9	1.16281	1.16566	1.15353	0.01213
1.0	1	1	1.00000	1.1102×10^{-16}

Table 3: Impact of β on coating thickness, separation point, force, and power input

β	λ	$\frac{H}{H_0}$	Separation point	Separation force	Power input
0	1.3015	0.6510	2.4102	−0.1345	−1.7315
0.01	1.3114	0.6560	2.4201	−0.7669	−1.8405
0.02	1.3214	0.6610	2.4301	−1.4044	−1.9497
0.03	1.3315	0.6660	2.4401	−2.0471	−2.0559
0.04	1.3414	0.6710	2.4501	−2.6950	−2.1613
0.05	1.3514	0.6760	2.4601	−3.3481	−2.2680
0.06	1.3612	0.6810	2.4701	−4.0064	−2.3779
0.07	1.3714	0.6860	2.4801	−4.6698	−2.4932
0.08	1.3813	0.6910	2.4900	−5.3383	−2.6158
0.09	1.3916	0.6960	2.5000	−6.0121	−2.7483

results and absolute errors were emphasized through diagrams and tables. All these numeric calculations have been calculated at the fixed value of the pressure gradient.

Figure 2 has been drawn to show the compression between Newtonian, analytical, and numerical outcomes for velocity for the various values of β. Numerical results are depicted with solid lines (black), while solid boxes (red)

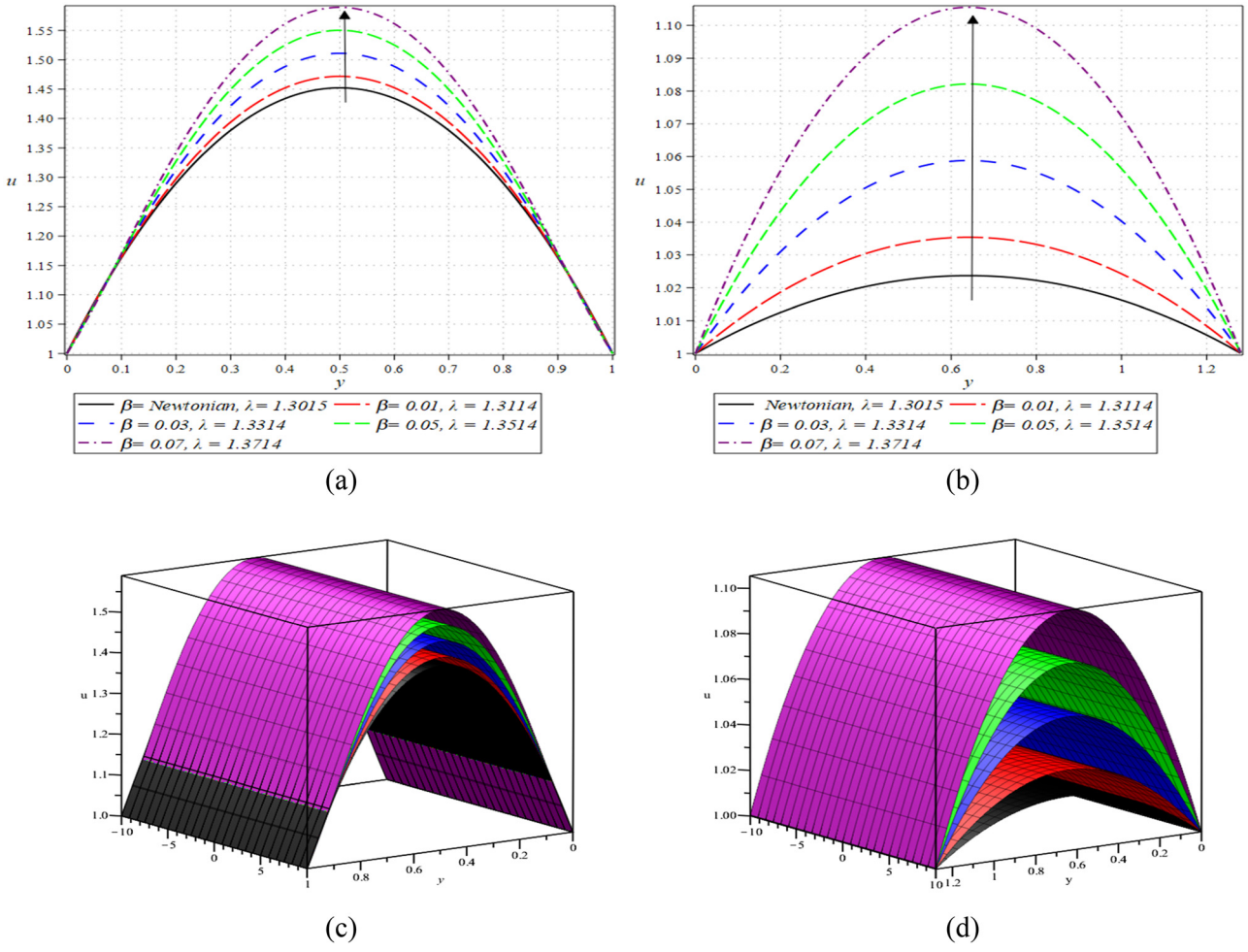

Figure 3: Impact of β on velocity profile in 2D and 3D view. (a) Velocity at $x = 0$, (b) velocity at $x = 0.75$, (c) 3D view of velocity at $x = 0$, and (d) 3D view of velocity at $x = 0.75$.

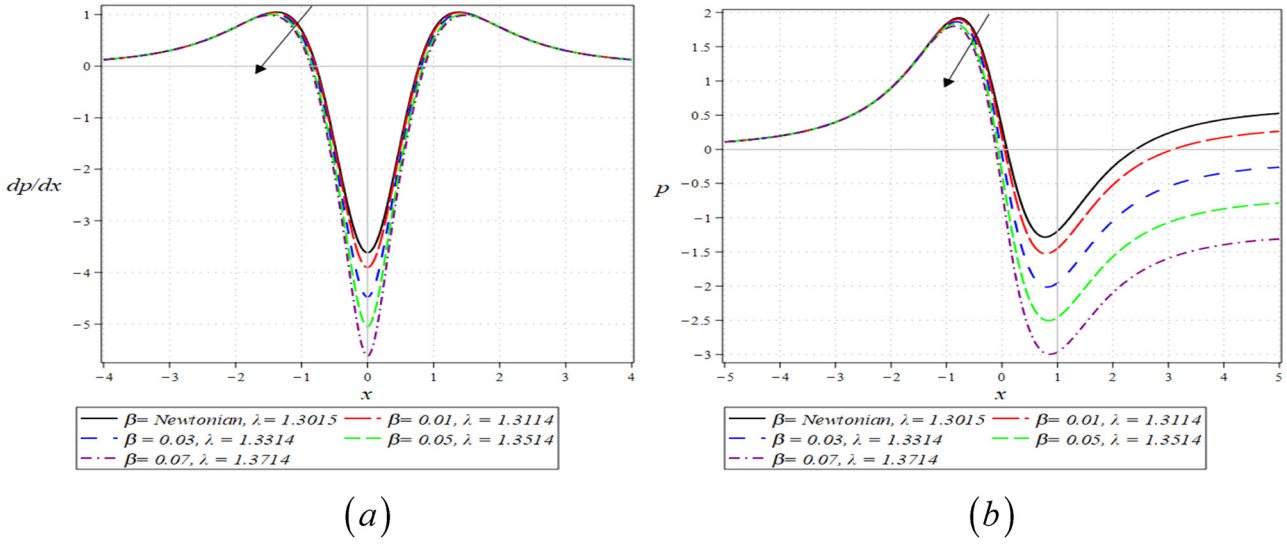

(a) (b)

Figure 4: Impact of β on (a) pressure gradient and (b) pressure profile.

and solid circles (purple) represent Newtonian and perturbed results. These graphs demonstrate a significant correlation among all solutions.

In addition, Tables 2 and 3 represent the approximate solution for velocity, calculated using perturbation and numerical methods for different values of involved parameters, and their absolute errors are also calculated. We can perceive reasonable agreement among the Newtonian, numerical, and analytical solutions. It exhibits that our technique and accompanying computations are valid (Table 1).

8 Results and discussion

This study inspected the rollover-web coating procedure for an incompressible Sisko fluid model. The LAT is used to simplify the motion equations. This study examines the influence of several parameters on critical factors like pressure gradient, streamline patterns, pressure distribution, velocity profiles, power input, and separation forces. The numerical results for essential variables, such as separation point x_s, volumetric flow rate λ, power

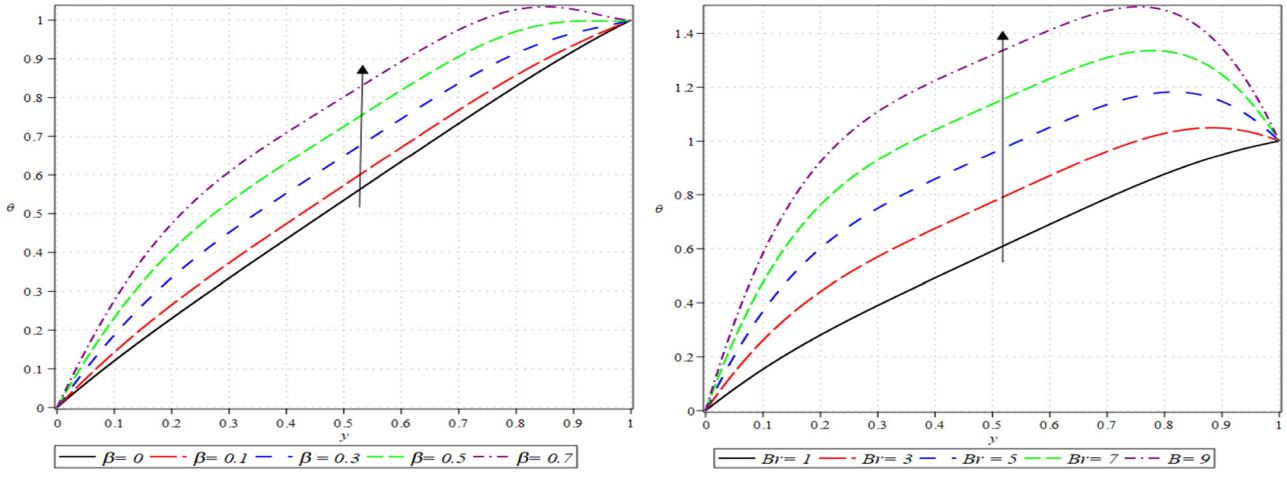

(a) (b)

Figure 5: Impact of β and Brinkman number on temperature profile. (a) Temperature for β and (b) temperature for Br.

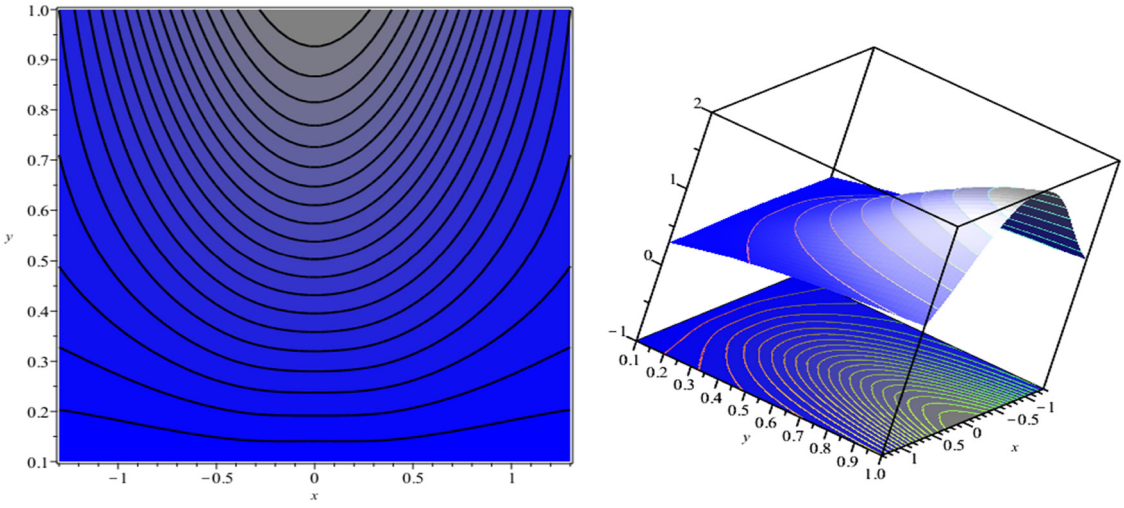

Figure 6: 2D and 3D view of streamline pattern for $\beta = 0.01$.

contribution p_w, Nusselt number Nu, exit sheet thickness $\frac{H}{H_0}$, and roll separating force F, were obtained using Maple 22 software. These results are tabulated in Table 3 for various Weissenberg values β. One notable discovery is the determination of an ideal separation point, accompanied by the observation of a maximum coating thickness of 0.6960 when the value of β approaches 0.9. There is a clear correlation between a rise in the values of β and an increase in the thickness of the coating. Whereas, when the value of β approaches zero, it is observed that the coating thickness reaches a minimum value of 0.6510. Significantly, the parameters of coating thickness, volume flow rate, and separation point demonstrate a progressive increase as β evolves.

Figure 3 illustrates the dimensionless velocity profiles at numerous stages within the RCP, highlighting the fluctuations in β. These graphs demonstrate a positive correlation between β and the fluid velocity, indicating that an increase in β leads to a proportional rise in the fluid velocity. Physically, it means that for higher values of β, the fluid viscosity begins to decrease, and thus, the fluid becomes less viscous owing to which the particles are free to move, and the velocity increases gradually.

Figure 4(a) demonstrates the pressure gradient $\frac{dp}{dx}$ *vs* x for increasing value of non-Newtonian parameters. The plot gives three separate regions, labeled as upstream region with $\frac{dp}{dx} > 0$, nip region with $\frac{dp}{dx} < 0$, and

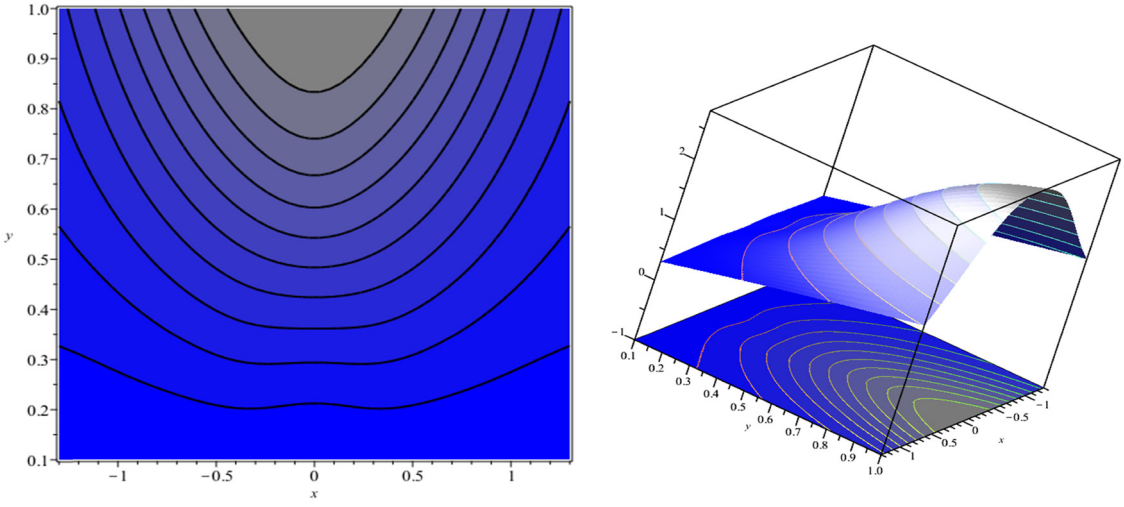

Figure 7: 2D and 3D view of streamline pattern for $\beta = 0.05$.

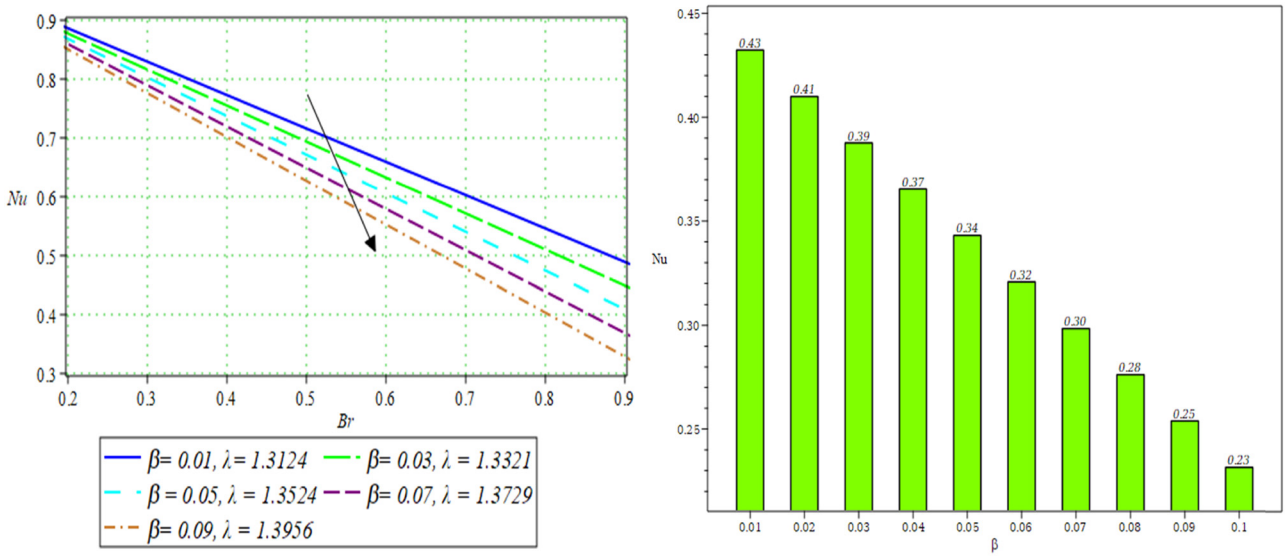

Figure 8: Nusselt number for β.

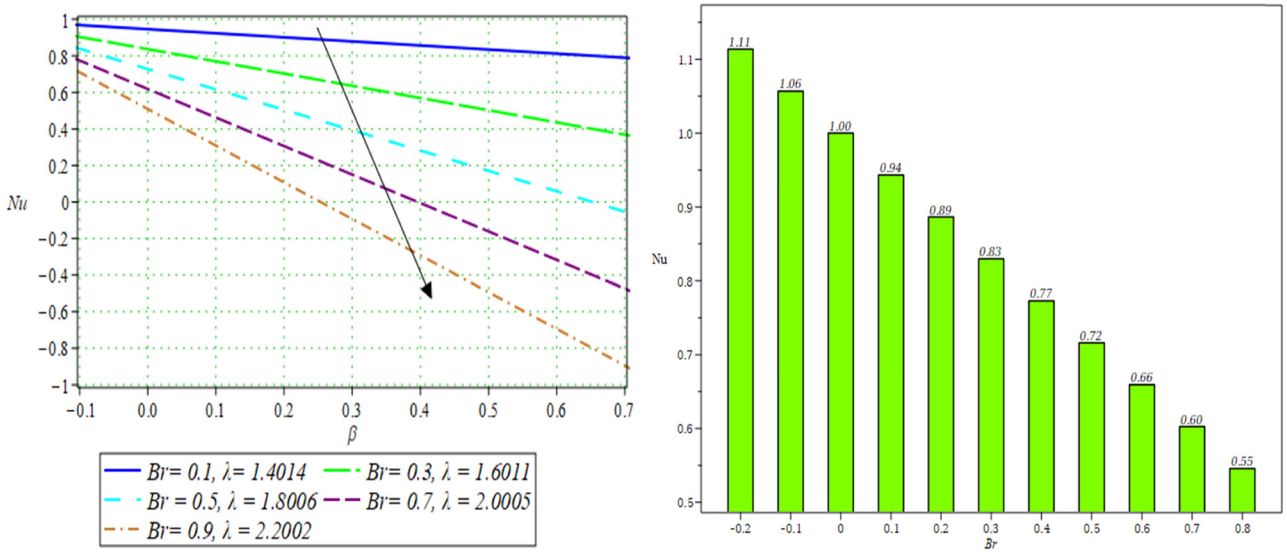

Figure 9: Nusselt number for Br.

downstream region with $\frac{dp}{dx} > 0$. In both the upstream and downstream zones, the $\frac{dp}{dx}$ serves as a hindrance to the flow. However, within the nip zone, it assumes a critical function in aiding the drag flow that is generated by the movement of the roll and sheet. It is worth noting that a rise in the non-Newtonian fluid parameter leads to a decrease in this phenomenon. The pressure profile, which lacks dimensional units, as depicted in Figure 4(b), offers significant insights regarding this phenomenon. It becomes apparent that with an increase in β, there is a discernible reduction in the pressure distribution. It is noticeable that the pressure reaches its peak just before reaching the nip. This is logically true because the maximum pressure is necessary to pass the fluid through narrow channels like the nip. Notably, the Newtonian curve, which corresponds to the scenario when β is assigned a value of zero, agrees with the findings previously documented by Middleman [6].

The visual representation of the impact of β and the Brinkman number Br upon the temperature profile may be observed in Figure 5(a and b). The pictures presented significantly contribute to our understanding of the thermal dynamics shown by the system. It is worth noting that a

comparable increase in temperature accompanies a rise in the parameter β. Increasing values of β causes a decrease in the viscosity of the fluid and creates more disturbance in the fluid particles, as a result of which temperature increases. Similarly, an increase in the Br also produces a similar effect. The Br is a dimensionless quantity that quantifies the relative contributions of heat created by viscous dissipation and heat carried by molecular conduction. Elevated values of the Br number indicate a diminished rate of heat conduction resulting from viscous dissipation, resulting in a more pronounced increase in temperature.

We provide visual representations of streamline patterns in two and three dimensions to depict fluid flow characteristics, as shown in Figures 6 and 7, respectively. Streamlines are essentially the trajectories followed by hypothetical particles suspended within a fluid and moving according to the fluid's motion. In this analysis, we examine the phenomenon of steady flow, wherein the streamlines remain stationary as the fluid undergoes motion. Variations in fluid velocity are observable when streamlines either closely converge or diverge, indicating regions of high and low fluid speeds, respectively. The impact of non-Newtonian parameters on Nusselt numbers has been shown in Figures 8 and 9. From the Figures, it has been observed that the Nusselt number is a decreasing function of non-Newtonian parameters.

9 Conclusion

This study encompasses a thorough theoretical investigation of the coating process (rollover-web), employing the Sisko fluid model. The methodology employed in our study consisted of converting non-dimensionalized nonlinear ordinary differential equations (ODEs) into more simplified forms by utilizing the LAT. We used the conventional perturbation technique to solve these refined nonlinear ODEs. The present study examined the complex relationship between physical parameters and critical factors, including velocity components, temperature distribution, flow rate, Nusselt number, power contribution, pressure profile, separation point, roll separating force, and required coating thickness. The primary outcomes of this investigation can be succinctly outlined as follows:

- An elevated non-Newtonian parameter results in a rise in fluid flow velocity.
- The temperature distribution increases by increasing the value of Br number.
- The non-Newtonian parameter causes a drop in pressure and pressure gradient within the nip zone.
- It has been noted that coating thickness increases with the Sisko fluid parameter.
- It has been observed that 2D and 3D streamline patterns are associated with the geometry of the problem which justify the fluid flow direction.
- A reasonable correlation has been found among Newtonian, analytical, and numerical solutions.
- The Newtonian solution is achieved when the dimensionless parameter becomes zero [6].

10 Further extension

Considering the slip and MHD effect in the isothermal fluid flow problem, two or more fluid layers can be used to handle future challenges.

Acknowledgments: This work was supported by the Deanship of Scientific Research, Vice Presidency for Graduate Studies and Scientific Research, King Faisal University, Saudi Arabia [Grant No. 6166], and the Talent Project of Tianchi Doctoral Program in Xinjiang Uyger Autonomous Region of China.

Funding information: This work was supported by the Deanship of Scientific Research, Vice Presidency for Graduate Studies and Scientific Research, King Faisal University, Saudi Arabia [Grant No. 6166].

Author contributions: Fateh Ali: conceptualization, mathematical modeling, solution methodology, writing – original draft, and software; M Zahid: discussion, writing, review – editing; Basma Souayeh: review – editing, English correction, and funding; Farwa Asmat: writing the original draft; Chinedu Nwaigwe: review – editing and software. All authors have accepted responsibility for the entire content of this manuscript and approved its submission.

Conflict of interest: The authors state no conflict of interest.

Data availability statement: Data sharing is not applicable to this article as no datasets were generated or analysed during the current study.

References

[1] Barbati AC, Desroches J, Robisson A, McKinley GH. Complex fluids and hydraulic fracturing. Annu Rev Chem Biomol Eng. 2016;7:415–53.

[2] Silva JA, Crimi M, Palaia T, Ko S, Davenport S. Field demonstration of polymer-amended in situ chemical oxidation (PA-ISCO). J Contam Hydrol. 2017;199:36–49.
[3] Xie C, Lv W, Wang M. Shear-thinning or shear-thickening fluid for better EOR? – A direct pore-scale study. J Pet Sci Eng. 2018;161:683–91.
[4] Nazeer M, Irfan M, Hussain F, Siddique I. Entropy generation analysis in blood-gold casson nanofluid through horizontal wavy channel with velocity and thermal slips: applications in skin diseases. J Comput Biophys Chem. 2023;22:259–72.
[5] Singh BK, Kumar A. New approximate series solutions of conformable time–space fractional Fokker–Planck Equation via two efficacious techniques. Partial Differ Equation Appl Maths. 2022;6:100451.
[6] Greener Y, Middleman S. A theory of roll coating of viscous and viscoelastic fluids. Polym Eng & Sci. 1975;15:1–10.
[7] Benkreira H, Patel R, Edwards M, Wilkinson W. Classification and analyses of coating flows. J Non-Newtonian Fluid Mech. 1994;54:437–47.
[8] Sofou S, Mitsoulis E. Roll-over-web coating of pseudoplastic and viscoplastic sheets using the lubrication approximation. J Plastic Film Sheeting. 2005;21:307–33.
[9] Zafar M, Rana M, Zahid M, Malik M, Lodhi M. Mathematical analysis of roll coating process by using couple stress fluid. J Nanofluids. 2019;8:1683–91.
[10] Ali F, Hou Y, Feng X. Backpropagation of Levenberg–Marquardt artificial neural networks for reverse roll coating process in the bath of Sisko fluid. Eur Phys J Plus. 2023;138:944.
[11] Aich W, Abbas T, Sewify GH, Sadiq MN, Khan SU, Bilal M, et al. Comparative numerical and analytical computations for magnetized pseudoplastic material with roll-coating applications. Alex Eng J. 2023;79:538–44.
[12] Middleman S. Fundamentals of polymer processing. 1977.
[13] Decré M, Gailly E, Buchlin JM. Meniscus shape experiments in forward roll coating. Phys Fluids. 1995;7:458–67.
[14] Lécuyer H, Mmbaga J, Hayes RE, Bertrand F, Tanguy PA. Modelling of forward roll coating flows with a deformable roll: Application to non-Newtonian industrial coating formulations. Comput Chem Eng. 2009;33:1427–37.
[15] Ali F, Hou Y, Zahid M, Rana MA. Mathematical analysis of pseudoplastic polymers during reverse roll-coating. Polymers. 2020;12:2285.
[16] Zahid M, Zafar M, Rana MA, Lodhi MS, Awan AS, Ahmad B. Mathematical analysis of a non-Newtonian polymer in the forward roll coating process. J Polym Eng. 2020;40:703–12.
[17] Manzoor T, Zafar M, Iqbal S, Nazar K, Ali M, Saleem M, et al. Theoretical analysis of roll-over-web surface thin layer coating. Coatings. 2020;10:691.
[18] Gaskell P, Innes G, Savage M. An experimental investigation of meniscus roll coating. J Fluid Mech. 1998;355:17–44.
[19] Atif HM, Ali N, Javed MA, Abbas F. Theoretical analysis of roll-over-web coating of a micropolar fluid under lubrication approximation theory. J Plastic Film Sheeting. 2018;34:418–38.
[20] Sisko A. The flow of lubricating greases. Ind Eng Chem. 1958;50:1789–92.
[21] Naz R, Noor M, Javed M, Hayat T. A numerical and analytical approach for exploration of entropy generation in Sisko nanofluid flow having swimming microorganisms. J Therm Anal Calorim. 2021;144:805–20.
[22] Shilpa B, Chandrashekhar D, Dinesh P, Vinay C, Raghavendra C, Gireesha B. Soret and Dufour effect on convection flow of Casson fluid in a channel. J Therm Anal Calorim. 2022;147:14939–51.
[23] Ali F, Hou Y, Zahid M, Rana M, Kumam P, Kanwal M, et al. Perturbation based analytical and numerical solutions of non-Newtonian differential equation during reverse roll coating process under lubrication approximation theory. Phys Scr. 2022;97:115203.
[24] Sanil P, Gudekote M, Choudhari R, Vaidya H, Prasad KV. Heat transfer analysis on peristaltic transport of Sisko fluid in an inclined uniform channel. J Adv Res Fluid Mech Therm Sci. 2023;103:157–79.
[25] Shakya G, Chaudhuri S, Sahoo S. Numerical and analytical investigation on pressure and shear driven flow of Sisko fluid. Proceedings of Conference on Fluid Mechanics and Fluid Power. Springer; 2021.
[26] Palencia JLD, Rahman S, Redondo AN. Regularity and reduction to a Hamilton-Jacobi equation for a MHD Eyring-Powell fluid. Alex Eng J. 2022;61:12283–91.
[27] Rahman S, Díaz Palencia JL, Roa González J. Analysis and profiles of travelling wave solutions to a Darcy-Forchheimer fluid formulated with a non-linear diffusion. AIMS Mathes. 2022;7:6898–914.
[28] Khanfer A, Bougoffa L, Bougouffa S. Analytic approximate solution of the extended blasius equation with temperature-dependent viscosity. J Nonlinear Math Phys. 2023;30:287–302.
[29] Cox BJ, Hill JM. Flow through a circular tube with a permeable Navier slip boundary. Nanoscale Res Lett. 2011;6:1–9.
[30] Ascher UM, Petzold LR. Computer methods for ordinary differential equations and differential-algebraic equations. Vol. 61, USA: Siam; 1998.